

PCCP

Accepted Manuscript



This is an *Accepted Manuscript*, which has been through the Royal Society of Chemistry peer review process and has been accepted for publication.

Accepted Manuscripts are published online shortly after acceptance, before technical editing, formatting and proof reading. Using this free service, authors can make their results available to the community, in citable form, before we publish the edited article. We will replace this *Accepted Manuscript* with the edited and formatted *Advance Article* as soon as it is available.

You can find more information about *Accepted Manuscripts* in the [Information for Authors](#).

Please note that technical editing may introduce minor changes to the text and/or graphics, which may alter content. The journal's standard [Terms & Conditions](#) and the [Ethical guidelines](#) still apply. In no event shall the Royal Society of Chemistry be held responsible for any errors or omissions in this *Accepted Manuscript* or any consequences arising from the use of any information it contains.

Activating and tuning basal planes of MoO₂, MoS₂, and MoSe₂ for hydrogen evolution reaction

Shi-Hsin Lin* and Jer-Lai Kuo†

Institute of Atomic and Molecular Sciences, Academia Sinica, Taipei, Taiwan

We investigated the defected two-dimensional materials MoX₂ (X = O, S, Se) for hydrogen evolution reaction by first principles calculations. While the basal plane is inert for pristine MoX₂, we found that the defected MoX₂ can adsorb hydrogen atoms at defect sites, with appropriate adsorption energies for hydrogen evolution. By analyzing density of states and charge density, we showed that a dangling bond state slightly below Fermi energy emerges when a defect is created. We proposed that this state is responsible for hybridizing with the hydrogen atom 1s state and hence the adsorption. Knowing the mechanism, we further considered tuning the reaction by adatoms (several first-row transition metals, B, C, N, O). We found that C and O adatoms can make defected MoX₂ ideal for hydrogen evolution at higher defect level (H coverage).

I. INTRODUCTION

Hydrogen has been anticipated to be one of the future clean energy sources, which has light weight, high energy density, and in the mean time, being earth abundant, and yet sustainable. The process that generates hydrogen molecules, hydrogen evolution reaction (HER), thus attracts a plethora of research efforts. Efficient and stable catalysts, such as Pt, are desirable. However, Pt is rare and expensive, therefore many of the efforts have been made to search inexpensive alternatives.

Recently, several transition metal dichalcogenides¹⁻⁷, such as MoS₂⁸⁻¹⁴, have been proposed to be very effective catalysts for HER with much lower costs than noble metals. For 2H-MoS₂, the reaction rate per site surpasses that of other common metals, and is slightly smaller than Pt. The edge sites of the MoS₂ nanosheets are found to be responsible for the HER⁹, with optimal operation at the H coverage of about one-quarter. Compared to Pt, which can operate at a H coverage around 1ML, the overall performance of MoS₂ thus can still not rival that of Pt. The strategies that have been undertaken include fabricating artificial structures to expose more edges with state-of-the-art technologies^{2,11}, and tuning the chemistry of the edge sites, to either make it more active or make the optimal condition at higher H coverage. For example, interlayer doping¹⁵ and different substrates¹⁶ can have impact on the activity of the edge sites. It is nevertheless hard to beat the number of active sites of a Pt surface, if the basal planes of the two-dimensional (2D) sheet are catalytically inert. Although the other thermodynamically metastable phase 1T-MoS₂ was shown to have an active basal plane^{12,17}, it transforms back to the energetically more stable 2H-MoS₂ on heating and aging¹⁸ and the phonon dispersion also suggests that 1T phase is not stable¹⁹. We have addressed the HER using 1T' phase, a reconstruction of 1T phase, of MX₂ (M = Mo, W; X = S, Se, Te) in another work²⁰. Here we therefore would like to explore whether the basal plane of 2H-MoS₂ (hereafter referred as MoS₂) can be activated to boost the overall reaction rate towards pragmatic commercial scale application.

At the edge sites of MoS₂, the translational symmetry is broken, and the orbital hybridization and the corresponding density of states and chemistry would differ from that of its bulk. For example, the (10 $\bar{1}$ 0) Mo-edge has smaller S/Mo ratio compared to the bulk counterpart (catalytically inert) and is catalytically reactive⁸. We hence investigated the HER at S defects of basal planes, wherein the translation symmetry is also broken with smaller S/Mo ratio. Defected MoS₂ can present in amorphous samples¹³, which is readily available for large scale production. Moreover, the defect level can be experimentally controlled by applying H₂ plasma treatment, making this proposal of immediate relevance to experiments and applications. We further extended our calculations to MoX₂ (X = O, S, Se) family, and illustrated the microscopic mechanism responsible for the HER efficiency. Based on the revealed mechanism, we addressed the utilization of adatoms to alter the material properties. Hence in this work, we predicted the basal planes of MoX₂ can be activated by creating defects, and in the mean time, we suggested that adatoms can be utilized to tune up the performance.

It has been demonstrated with density functional calculations²¹ that a smaller absolute value of the free energy difference between the intermediate and final state corresponds to a greater HER efficiency. Therefore in this work we calculated the free energy difference ΔG of the intermediate (H atom adsorbed on MoS₂) and final state (MoS₂ and free H₂) obtained via²¹:

$$\Delta G = \Delta E + \Delta E_{ZPE} - T\Delta S, \quad (1)$$

where ΔE is the differential hydrogen chemisorption energy, ΔE_{ZPE} is the zero point energy difference between the adsorbed state and the molecular state, T is the temperature (room temperature adopted in this work) and ΔS is the entropy difference between these two states, which has been discussed in Ref. 21. We calculated the differential hydrogen chemisorption energy by:

$$\Delta E = \frac{1}{n} \left(E[\text{MoS}_2 + n\text{H}] - E[\text{MoS}_2] - \frac{n}{2} E[\text{H}_2] \right), \quad (2)$$

where $E[\text{MoS}_2 + n\text{H}]$ is the energy of MoS_2 with n adsorbed hydrogen atoms, $E[\text{MoS}_2]$ is the energy of MoS_2 , and $E[\text{H}_2]$ is the energy of the hydrogen molecule. The zero point energy is obtained by summing over the vibrational modes of the H adsorbed on MoS_2 .

In Sec. II, we outlined the computation methods employed. We illustrated our results of defected MoO_2 , MoS_2 , and MoSe_2 in Sec. III, and analyzed the mechanism of binding H atom. Knowing the mechanism, we further demonstrated that adatoms can improve the HER efficiency by increasing the optimal H coverage of defected MoS_2 .

II. METHOD

We performed density functional calculations with projector-augmented-wave (PAW) potentials^{22,23} using the Vienna ab initio simulation package (VASP)^{24,25}, where generalized gradient approximation (GGA) in Perdew-Burke-Ernzerhof (PBE)²⁶ format were adopted as the exchange correlation functionals. A plane wave cutoff energy 460 eV were used together with the Brillouin zone sampling $4 \times 4 \times 1$ k -point grid centered at the Γ point. A 15 Å vacuum layer was inserted to reduce the artificial interlayer coupling. The structures were relaxed with the conjugate gradient method with the force less than 0.01 eV/Å. The obtained lattice constants for MoO_2 , MoS_2 , and MoSe_2 are 2.81, 3.18 and 3.32 Å respectively. We adopted DFT-D2 method²⁷ to account for the Van der Waals interaction through our calculations.

III. RESULTS

A. activate basal plane of MoX_2 by creating defects

We calculated the Gibbs free energy difference for pristine and defected MoX_2 at various defect levels, as shown in Table I. 4×4 supercells were used throughout this work and the geometries of a pristine and defected MoS_2 with a hydrogen atom adsorbed were shown in Fig. 1. S atoms were removed to create S defects. For the pristine cases, the free energy differences are all greater than 2 eV, comparable to half of the hydrogen molecule dissociation energy, suggesting that the pristine MoX_2 barely adsorb hydrogen atoms. The resulting free energies of the intermediate state (the adsorbed H atom) are too high so that the pristine MoX_2 are all inert for HER. This conclusion drawn from our first-principles calculations is consistent with previous experimental findings⁹, wherein the HER activities are correlated with the edge dimensions. Meanwhile, once defects are created, the free energy differences are reduced significantly for all three MoX_2 . This indicates much enhanced H adsorptions on MoX_2 , which mechanism will be discussed later.

For certain defect levels, such as $\text{MoS}_{2-0.0625}$, and $\text{MoO}_{2-(0.0625 \text{ to } 0.25)}$, the free energy differences are

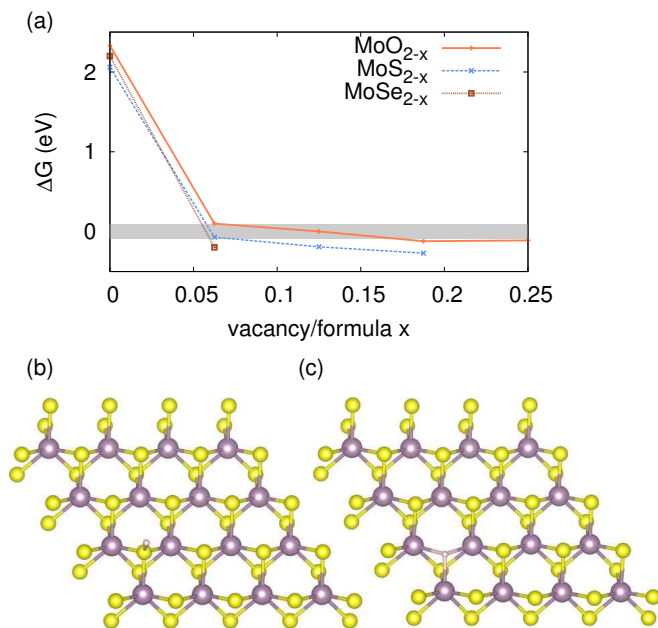


FIG. 1. The Gibbs free energy difference $\Delta G = \Delta E + \Delta E_{ZPE} - T\Delta S$ for pristine and defected MoX_2 at various defect levels are shown in (a), calculated by PBE functional with dispersion correction. The shaded area is $\pm |\Delta G|$ of Pt for adsorbate coverage $1/4$ ²¹. The creation of defects greatly enhances the hydrogen atom adsorption and hence the HER. The geometries of a pristine and defected MoS_2 (Mo: purple ball, S: yellow ball) with a hydrogen atom (H: white ball) adsorbed are shown in (b) and (c). Hydrogen is adsorbed at the defect site for defected MoS_2 .

	x	ΔE (eV)	$\Delta E_{ZPE} - T\Delta S$ (eV)	ΔG (eV)
MoO_{2-x}	0	+2.25	0.08	+2.33
	0.0625	-0.14	0.25	+0.11
	0.1250	-0.24	0.25	-0.00
	0.1875	-0.35	0.23	-0.12
	0.2500	-0.36	0.25	-0.11
MoS_{2-x}	0	+1.84	0.22	+2.06
	0.0625	-0.29	0.22	-0.07
	0.1250	-0.41	0.22	-0.19
	0.1875	-0.49	0.22	-0.27
	0.2500	-0.41	0.22	-0.19
MoSe_{2-x}	0	2.04	0.16	2.20
	0.0625	-0.40	0.21	-0.20

TABLE I. The Gibbs free energy difference $\Delta G = \Delta E + \Delta E_{ZPE} - T\Delta S$ for pristine and defected MoX_2 at various defect levels. For certain defect levels, such as $\text{MoS}_{2-0.0625}$, and $\text{MoO}_{2-(0.0625 \text{ to } 0.25)}$, the free energy differences are nearly vanishing, making the corresponding defected MoX_2 highly effective for HER. (Two of the frequencies of the vibrational modes for MoO_2 are imaginary.)

nearly vanishing, making the corresponding defected MoX_2 highly effective for HER. This can shed light on the recent experimental finds that amorphous MoS_3 shows

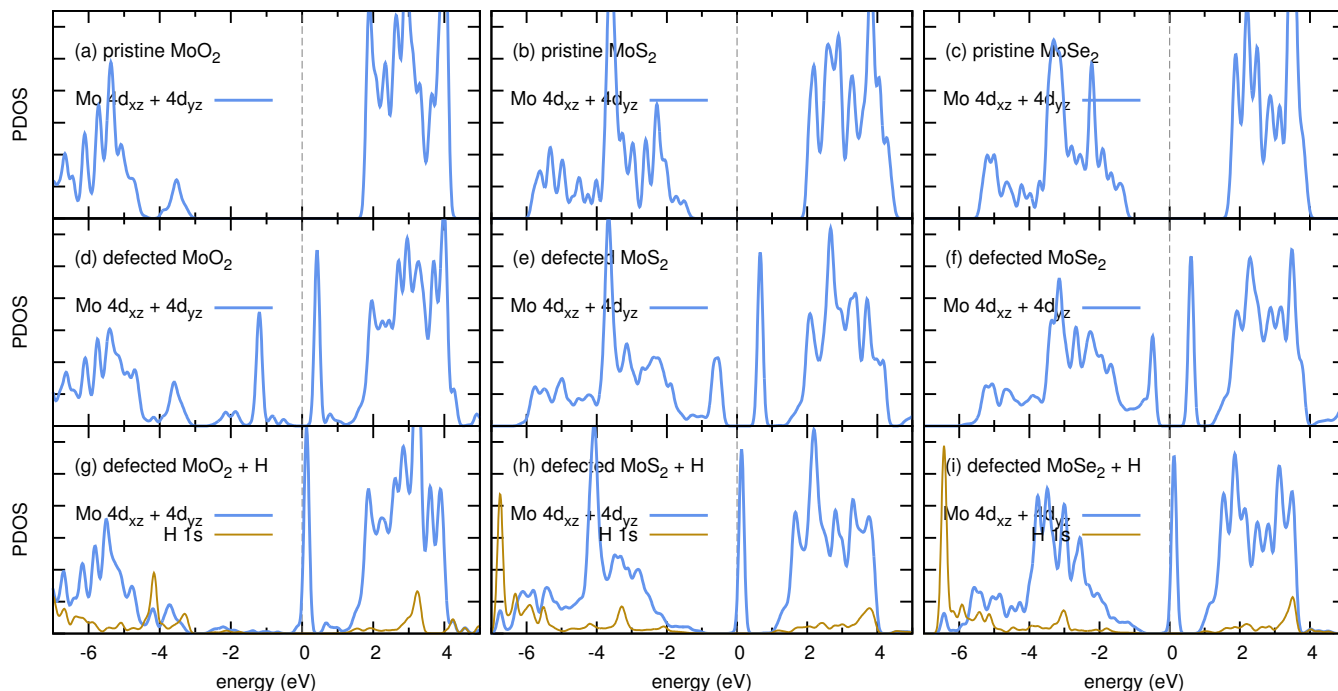


FIG. 2. Projected density of states prior to the H adsorption of pristine (a) MoO₂, (b) MoS₂, and (c) MoSe₂, defected (d) MoO₂, (e) MoS₂, and (f) MoSe₂ and posterior to the H adsorption of defected (g) MoO₂, (h) MoS₂, and (i) MoSe₂.

better HER catalytic activity than polycrystalline and single crystalline MoS₂ and MoS₃ particles²⁸. As more defects are created, the adsorptions are further enhanced for all MoX₂ systems. The adsorptions are eventually too strong, causing reduction of HER efficiency. Comparing oxides, sulfide, and selenide, for a 4×4 supercell, MoO₂ has the weakest adsorption energy for one defect and therefore is efficient for HER at higher defect levels (4 defects). MoS₂ is ideal only for one defect. The adsorption of hydrogen atoms on MoSe₂ is too strong for the purpose of HER, and thus might only be applicable at even lower defect level. We concluded that suitable defect levels for MoX₂ should be adopted and can be achieved experimentally by controlling the H₂ plasma treatment time. Among the MoX₂, MoO₂ can function at higher H coverage than MoS₂, and is suggested to attribute to the excellent performance of amorphous samples²⁹.

To elucidate the adsorption mechanism, we analyzed the projected density of states (PDOS), as shown in Fig. 2. Prior to the adsorption, the PDOS of defected MoS₂ shows one peak above the Fermi energy and one peak below, which are absent in pristine MoS₂. Posterior to the adsorption, the peak below the Fermi energy disappears, suggesting that this peak of states is responsible for hybridizing with H 1s orbitals. The hybridization mixes this peak of states and H 1s, and leads to further split anti-bonding and bonding states. If the hybridization is strong enough or the states participated are close enough to Fermi energy, the formed anti-bonding states can be shifted above the Fermi level. As a result, the electrons fill only the bonding states and the energy of the

system is lowered, which is the adsorption energy gain. Hence defects can switch on the H adsorption. As such peaks of states slightly below Fermi energy are absent in pristine MoS₂, pristine MoS₂ is not capable of binding H. It is demonstrated by the large free energy difference discussed above. This feature of PDOS is found in all three MoX₂, and all defected MoX₂ can adsorb H much stronger than pristine ones. Similar analysis on DOS had been proposed for transition metal catalysts, wherein *d* band center was adopted as a descriptor^{30–32}.

The two peaks that are missing in pristine MoS₂ correspond to dangling bond states (Mo *d* orbitals) when creating S defects. They are localized in the vicinity of defect sites. We further calculated the band structures of pristine and defected MoS₂, and the partial charge densities of these two localized bands, shown in Fig. 3. The two emerging flat bands in Fig. 3(b), which are the two peaks shown in PDOS, have very different charge density distributions. The charge density of the band above the Fermi level is vanishing at the defect site (Fig. 3(c)), while that of the band below is characterized by a triangular shape centered at the defect (Fig. 3(d)). It is consistent with the picture discussed in the paragraph above regarding the PDOS (Fig. 2), the former peak is almost intact after adsorption, and does not participate in the hybridization since its wave function does not overlap with H 1s well. The latter peak, nevertheless, is largely modified as its wave function overlaps with that of H 1s, which results in the hybridization and modification of PDOS.

Regarding the comparison of MoO₂, MoS₂, and MoSe₂,

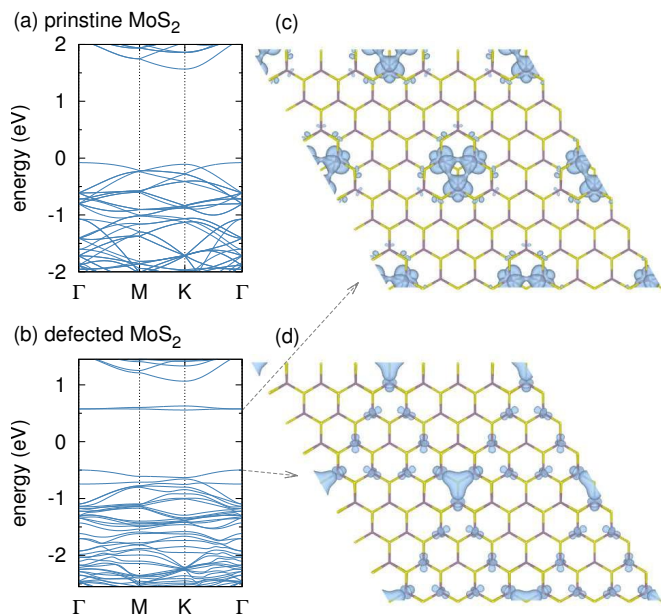


FIG. 3. Band structure of pristine MoS₂ is shown in (a), defected MoS₂ (one defect) in (b). (c) and (d) show the charge densities of the two flat dangling bond bands, above and below Fermi energy.

the PDOS of MoO₂ below Fermi energy spread more sparsely than the others, likely attributing to the weaker adsorption at the same defect level. On the contrary, the PDOS of MoSe₂ below Fermi energy is squeezed more towards the Fermi energy and the dangling bond peak below Fermi energy has a slightly wider shoulder than MoS₂. As a result, it could lead to a stronger hybridization and consequently stronger adsorption than MoS₂. Therefore our PDOS analysis suggests that reducing those peak of states below Fermi energy can in principle weaken the adsorption such that the ideal free energy difference can be achieved at higher H coverage. We have further exploited this approach and discussed in the next section.

B. tuning HER with adatoms

Following the last paragraph, to enhance HER, there can be several ways to reduce or perturb the states below Fermi energy, such as:

- substitution of elements: for example doping¹⁵ and, as we addressed in the previous section, substitution of S with O to increase the H coverage.
- substrates: substrates can fine tune the electronic structures as discussed in the case of MoS₂ edge¹⁶.
- strains: 2D materials are known to be able to sustain sizable strains. Hence strains can modify the electronic states effectively^{33–36}. It was reported for some systems⁴.

- adatoms or clusters: as we only need to alter the chemical environment locally near the defects, adatoms can be used to perturb those states near Fermi energy. This method can be relatively simple experimentally, and might even applicable to some amorphous samples, which can be of paramount importance to industrial scale production.

In this section, we therefore propose to utilize adatoms to tune HER, which to our knowledge haven't been reported.

In practical devices, 2D materials are deposited on substrates as electrodes. Au, highly ordered pyrolytic graphite, graphitic carbon, and carbon cloth have generally been adopted for the substrates. As lattice imperfection, defects are not unusual, there could be carbons with low coordination numbers interact with the supported 2D materials. On the other hand, during fabrication there are generally N₂ and O₂ in the chamber, and hence inevitably these molecules can interact with the 2D materials as well. Thus a suitable consideration of effects of adatoms is not only useful in tuning HER, but also necessary in terms industrial applications. It is also possible to disperse metals onto the 2D materials to alter the density of states near Fermi energy. We hence calculated the adsorptions of defected MoS₂ decorated with several types of transition metals (early, middle, and late), B, C, N, and O at various sites. These include (1) the S on the opposite side of the defect (S site), (2) the Mo adjacent to the defect, on the opposite side of the defect (Mo site), and (3) the hexagonal center site surrounding the defect (HEX site). The adsorption sites and energies ΔE_{ad} of the adatoms, and the corresponding adsorption energies and free energies of the hydrogen atom is shown in Table II and discussed below.

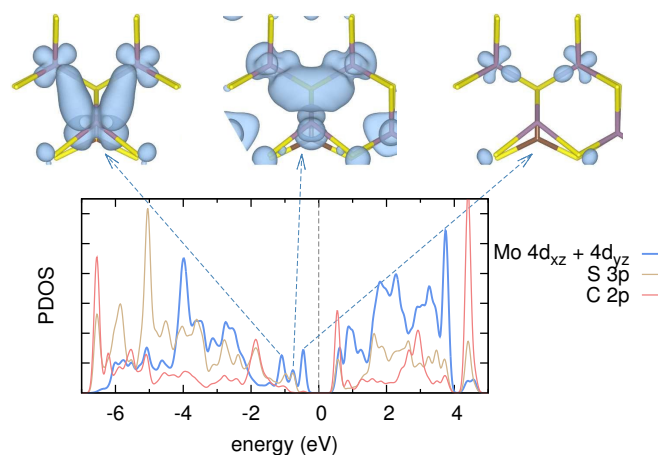


FIG. 4. PDOS at the S defect site of defected MoS₂ with C adatom under one of the adjacent Mo. The two dangling bond peaks near Fermi energy for defected MoS₂ (Fig. 2(e)) is split into three weaker peaks, and the resulting adsorption is weaker. The charge density distribution corresponding to these three peaks is shown above the plot.

adatom	site	ΔE_{ad} (eV)	ΔE (eV)	ΔG (eV)
Sc	Mo	-3.06	-0.38	-0.18
	Mo*	-1.62	-0.37	-0.17
Mn	hex	-1.52	+0.27	0.47
	Mo*	-4.07	-0.31	-0.09
Ni	S	-2.41	-1.70	-1.49
	Mo*	-0.22	-0.27	-0.06
Zn	S	-0.12	-0.27	-0.05
	hex	-0.18	-	-
	Mo*	-4.14	-0.89	-0.64
B	hex	-4.10	-1.44	-1.18
	Mo	-3.71	-0.12	+0.12
C	S	-2.24	-0.22	-0.01
	hex*	-4.26	-0.13	+0.12
	Mo	-1.20	-0.31	-0.07
N	S*	-1.71	-0.40	-0.17
	hex	-1.54	-0.57	-0.35
	O	-3.84	-0.10	+0.11

TABLE II. The Gibbs free energy difference $\Delta G = \Delta E + \Delta E_{ZPE} - T\Delta S$ for defected MoS₂ with various adatoms. We calculated by PBE functional with dispersion correction. ΔE_{ad} is the adsorption energy of the adatom, and the preferred adsorption site (lowest ΔE_{ad}) is marked with a superscript asterisk. Our calculations showed that C and O adatoms are effective in reducing the H adsorption and thus can make the defected MoS₂ operate at defect levels (higher H coverages).

We found C and O adatoms most effective in reducing the adsorption energy, thus possibly having ideal HER rate per site at higher coverage (defect level). C was found to be able to adsorb on S site, Mo site, and HEX site. When C is adsorbed below the S under defect, the adsorption energy is slightly reduced. It is due to that electrons of Mo are drawn to bind C, leaving less electrons for the binding hydrogen states. On the other hand, when adsorbed at Mo bottom and HEX sites the adsorption energy is much more reduced, as it more directly perturbs the Mo *d* orbitals. As seen from the PDOS and partial charge densities in Fig. 4, the two dangling bond peaks that can participate in adsorption are split into three weaker peaks. As less electrons can participate in binding H, reduced dangling bond states correspond to weaker adsorptions. At higher defect levels and more adatoms, the same mechanism, wherein adatoms perturb the dangling bond states, still holds. The effect could be lessened only if those adatoms interact with each other and form clusters, thus disturb the dangling bond state less. But still it will weaken, not enhance, the adsorption, compared to the materials without adatoms, and hence make the materials operating at higher, not lower, defect levels for HER. When C is adsorbed above the Mo (on the same side of the defect), the adsorption is enhanced. The peak of PDOS (not shown here) below the Fermi energy is shifted towards higher energy (still below

the Fermi level), and it leads to the enhancement of the adsorption. For O adatoms, the O can only be adsorbed on the S site. The corresponding free energy difference is comparable to that of MoS₂ with C adatoms on the Mo and HEX sites. It suggests that O attachments are beneficial to HER, thus the unavoidable oxidation in the fabrication chamber, can actually promote the performance of MoS₂. However, if the O is on the same side of the defect, O can fill the defect. As the reactive center, the defect, is removed, the HER efficiency is diminished. Therefore, the fabricated electrode should avoid to be exposed to the air.

When transition metals are dispersed on MoS₂, the effect on HER is found to be weak. The early and middle transition metals (Sc and Mn) can lead to a slightly stronger adsorption. With greater atomic numbers, late transition metals Ni and Zn barely modify the hydrogen adsorption of MoS₂.

IV. CONCLUSION

We proposed to activate the inert basal planes of MoX₂ (X = O, S, Se) by creating defects, and justified by first-principles calculations using PBE functional and DFT-D2 Van der Waals correction. We found that the recently popular 2D material MoS₂, if prepared with a suitable defect level (MoS_{2-x} with $x = 0.625$), can supply an adsorption free energy $\Delta G \approx 0$ for HER at basal planes. Consequently, the reactions can take place at not only edge sites, but also the activated basal plane defect sites, making the number of active sites much increased. For example, for a monolayer of MoS₂ with lateral size 5 nm, the number of active sites for a defected sample can be five times of that for a pristine one. For a sample with dimension *L*, the number of active sites scales with *L*² rather than *L* that is correlated with the edge sites in previous studies of pristine MoS₂. Therefore, larger samples, such as thin films and a few monolayers, can be advantageous. Moreover, we discovered that defected MoO₂ can function at even higher H coverage than MoS₂. Our PDOS analysis showed that a localized peak near Fermi energy emerges as the defect is created. It corresponds to the dangling bond localized at the defect, and is responsible for hybridizing with the H 1s orbital. We therefore further considered utilizing adatoms to perturb this peak to enhance HER. Our calculations showed that C and O adatoms are effective in reducing the H adsorption and thus can make the defected MoS₂ operate at higher defect levels (higher H coverages). Hence, we suggest that the inevitable oxidation during fabrication and amorphous carbon based substrates might be favorable for the enhancement of the HER efficiency. In short, this work predicted an experimentally accessible method to activate basal planes of MoX₂, which can furnish more active sites than edge sites of previously studied pristine MoS₂. In the mean time, we suggested that adatoms can help to tune up the performance.

ACKNOWLEDGMENTS

This work was financially supported by the Academia Sinica, the Ministry of Science and Technology (MOST) of Taiwan under MOST101-2113-M-001-023-MY3, and

the National Center for Theoretical Sciences Physics Division. Computational resources are supported in part by the National Center for High Performance Computing. We would like to thank Lain-Jong Li for valuable discussions. S.-H. Lin would also like to thank Ang-Yu Lu, and Chien-Chi Tseng for discussing experimental details.

- * slin2@gate.sinica.edu.tw
† jlkuo@pub.iams.sinica.edu.tw
- ¹ D. Kong, J. J. Cha, H. Wang, H. R. Lee, and Y. Cui, *Energy Environ. Sci.* **6**, 3553 (2013).
 - ² D. Kong, H. Wang, J. J. Cha, M. Pasta, K. J. Koski, J. Yao, and Y. Cui, *Nano Lett.* **13**, 1341 (2013).
 - ³ H. Wang, D. Kong, P. Johanes, J. J. Cha, G. Zheng, K. Yan, N. Liu, and Y. Cui, *Nano Lett.* **13**, 3426 (2013).
 - ⁴ D. Voiry, H. Yamaguchi, J. Li, R. Silva, D. C. B. Alves, T. Fujita, M. Chen, T. Asefa, V. B. Shenoy, G. Eda, and M. Chhowalla, *Nat. Mater.* **12**, 850 (2013).
 - ⁵ C. Tsai, K. Chan, F. Abild-Pedersen, and J. K. Nørskov, *Phys. Chem. Chem. Phys.* **16**, 13156 (2014).
 - ⁶ M. A. Lukowski, A. S. Daniel, C. R. English, F. Meng, A. Forticaux, R. J. Hamers, and S. Jin, *Energy Environ. Sci.* **7**, 2608 (2014).
 - ⁷ M. S. Faber and S. Jin, *Energy Environ. Sci.* **7**, 3519 (2014).
 - ⁸ B. Hinnemann, P. G. Moses, J. Bonde, K. P. Jørgensen, J. H. Nielsen, S. Horch, I. Chorkendorff, and J. K. Nørskov, *J. Am. Chem. Soc.* **127**, 5308 (2005).
 - ⁹ T. F. Jaramillo, K. P. Jørgensen, J. Bonde, J. H. Nielsen, S. Horch, and I. Chorkendorff, *Science (New York, N.Y.)* **317**, 100 (2007).
 - ¹⁰ Y. Li, H. Wang, L. Xie, Y. Liang, G. Hong, and H. Dai, *J. Am. Chem. Soc.* **133**, 7296 (2011).
 - ¹¹ J. Kibsgaard, Z. Chen, B. N. Reinecke, and T. F. Jaramillo, *Nat. Mater.* **11**, 963 (2012).
 - ¹² M. A. Lukowski, A. S. Daniel, F. Meng, A. Forticaux, L. Li, and S. Jin, *J. Am. Chem. Soc.* **135**, 10274 (2013).
 - ¹³ D. Merki, S. Fierro, H. Vrubel, and X. Hu, *Chem. Sci.* **2**, 1262 (2011).
 - ¹⁴ Y. Yan, B. Xia, Z. Xu, and X. Wang, *ACS Catal.* **4**, 1693 (2014).
 - ¹⁵ X. Sun, J. Dai, Y. Guo, C. Wu, F. Hu, J. Zhao, X. Zeng, and Y. Xie, *Nanoscale* **6**, 8359 (2014).
 - ¹⁶ C. Tsai, F. Abild-Pedersen, and J. K. Nørskov, *Nano Lett.* **14**, 1381 (2014).
 - ¹⁷ D. Voiry, M. Salehi, R. Silva, T. Fujita, M. Chen, T. Asefa, V. B. Shenoy, G. Eda, and M. Chhowalla, *Nano Lett.* **13**, 6222 (2013).
 - ¹⁸ D. Yang, S. Sandoval, W. Divigalpitiya, J. Irwin, and R. Frindt, *Phys. Rev. B* **43**, 12053 (1991).
 - ¹⁹ M. Calandra, *Phys. Rev. B* **88**, 245428 (2013).
 - ²⁰ D. Putungan, S.-H. Lin, and J.-L. Kuo, *Phys. Chem. Chem. Phys.* **17**, 21702 (2015).
 - ²¹ J. K. Nørskov, T. Bligaard, A. Logadottir, J. R. Kitchin, J. G. Chen, S. Pandalov, and U. Stimming, *J. Electrochem. Soc.* **152**, J23 (2005).
 - ²² P. E. Blöchl, *Phys. Rev. B* **50**, 17953 (1994).
 - ²³ G. Kresse and D. Joubert, *Phys. Rev. B* **59**, 1758 (1999).
 - ²⁴ G. Kresse and J. Hafner, *Phys. Rev. B* **48**, 13115 (1993).
 - ²⁵ G. Kresse, *Phys. Rev. B* **54**, 11169 (1996).
 - ²⁶ J. P. Perdew, K. Burke, and M. Ernzerhof, *Phys. Rev. Lett.* **77**, 3865 (1996).
 - ²⁷ S. Grimme, *J. Comput. Chem.* **27**, 1787 (2006).
 - ²⁸ H. Vrubel, D. Merki, and X. Hu, *Energy Environ. Sci.* **5**, 6136 (2012).
 - ²⁹ A.-Y. Lu, C.-C. Tseng, X. Yang, S.-H. Lin, S. Min, C.-L. Hsu, H. Li, J.-L. Kuo, K.-W. Huang, and L.-J. Li, to be submitted.
 - ³⁰ B. Hammer and J. K. Nørskov, *Surf. Sci.* **343**, 211 (1995).
 - ³¹ B. Hammer and J. K. Nørskov, *Adv. Catal.* **45**, 71 (2000).
 - ³² J. K. Nørskov, F. Abild-Pedersen, F. Studt, and T. Bligaard, *Proc. Natl. Acad. Sci. U. S. A.* **108**, 937 (2011).
 - ³³ C.-H. Chang, X. Fan, S.-H. Lin, and J.-L. Kuo, *Phys. Rev. B* **88**, 195420 (2013).
 - ³⁴ Y. Ma, Y. Dai, M. Guo, C. Niu, J. Lu, and B. Huang, *Phys. Chem. Chem. Phys.* **13**, 15546 (2011).
 - ³⁵ Y. Ma, Y. Dai, M. Guo, C. Niu, Y. Zhu, and B. Huang, *ACS Nano* **6**, 1695 (2012).
 - ³⁶ Y. Ma, Y. Dai, M. Guo, L. Yu, and B. Huang, *Phys. Chem. Chem. Phys.* **15**, 7098 (2013).